Thermal and Structural Aspect of the Hydride Conducting Oxyhydride La_2LiHO_3 obtained via a Halide Flux Method

Øystein S. Fjellvåg,[†] Jeff Armstrong,[‡] Wojciech A. Slawinski[‡] and Anja O. Sjåstad*,[†]

[†]Centre for Materials Science and Nanotechnology, Department of Chemistry, University of Oslo, POBox 1033, N-0315 Oslo, Norway

[‡]ISIS Facility, Rutherford Appleton Laboratory, Harwell Oxford, Didcot, Oxfordshire OX11 0QX, U.K.

Abstract

Oxyhydrides, in which oxide- and hydride- anions share the same anionic lattice, are relatively rare compounds. La_2LiHO_3 belongs to this family. We report the synthesis of La_2LiHO_3 by means of an alkali halide flux method, which allows the production of larger quantities of material relative to the usually adopted synthesis routes. Powder X-ray and neutron diffraction studies show that La_2LiHO_3 adopts the n = 1 Ruddlesden-Popper (RP) type structure with an orthorhombic distortion (space group *Immm*) due to hydride- and oxide-anion ordering. No sign of polymorphism is observed. La_2LiHO_3 is seen to decompose in an oxygen atmosphere at ~450 ^{o}C into $La_2LiO_{3.5}$. We show that the high mobility of hydride anions close to the decomposition temperature is likely the main factor in inducing the oxidation. The crystal structure of $La_2LiO_{3.5}$ is also determined, and takes an RP n = 1 type structure with an orthorhombic distortion (*Fmmm*). This newly reported large scale synthesis approach, combined with the proven high thermal stability, are key factors for potential practical applications of this oxyhydride in real devices.

Introduction

Hydrogen conducting materials have been widely studied for various technological applications. Examples include proton conductors [1], high temperature solid oxide fuel components and metals for hydrogen storage [2]. For the latter category, the monoatomic hydrogen is typically assigned to oxidation state zero, whereas in oxide based ceramics hydrogen is present as protons (H^+). With the electropositive elements, hydrogen takes formally oxidation state –1, which in compounds of ionic nature is manifested by hydride anions (H^-). In oxides the occurrence of H^- anions is rare, and such oxyhydrides are likely to have different chemical and physical properties than their proton bearing counterparts. This was recently demonstrated by Kobayashi *et al*. who showed pure H^- conductivity in the oxyhydride La_2LiHO_3 as well as documenting this functionality through a prototype solid state $Ti/La_2LiHO_3/TiH_2$ battery [3]. We foresee yet undiscovered oxyhydrides and their functional properties to have the promise of opening up a new dimension in materials chemistry.

Only a limited number of oxyhydrides in which the oxide- and hydride-anions are sharing the same anionic lattice have so far been reported. Most of the known oxyhydrides take the perovskite- (ABO_3: $BaTiH_xO_{3-x}$ [4], $SrVHO_2$ [5]) or the n = 1 Ruddlesden-Popper ($A_{n+1}B_nO_{3n+1}$: $Sr_2VH_xO_{4-x}$ [6], $LaSrCoH_{0.7}O_3$ [7]) type structure. In these compounds the two anions are basically occupying the same anionic sub-lattice either in an ordered or a disordered manner.

The synthesis of oxyhydrides is challenging. Reviewing the literature with respect to reported procedures, two routes stand out as the most adopted approaches; i) solid state ion-exchange with metal hydride and ii) direct solid state reaction at high pressure (GPa range). The RP (n = 1, RP1) like compound $LaSrCoH_{0.7}O_3$ was successfully synthesized via ion-exchange of the corresponding $LaSrCoO_{4-x}$ oxygen defect RP-type oxide by direct reaction with CaH_2 in a sealed, evacuated ampoule at intermediate temperatures (450 ^oC) [7]. The reaction is assumed to be facilitated by a significant vacancy concentration of the starting RP1 oxide [8]. The obtained oxyhydride products from this method are known to be non-stoichiometric with respect to H-content and the hydride- and oxide-anions are randomly distributed over the anionic lattice. Through direct reaction between hydride- and oxide-containing reactants at high pressure and moderate temperature, mixed anionic compounds such as La_2LiHO_3 [3] and $SrCrHO_2$ [9] are synthesized. An obstacle for this approach is the small (*mg*-range) quantity of material obtained in each batch, implying that producing sufficient material for prototype devices or for measurements of samples in the gram range becomes cumbersome. Only one single report exists on a totally different synthesis approach; *i.e*. via an alkali halide flux route [10]. In this respect La_2LiHO_3 was for the first time reported in 1991 by Schwarz [10], where La_2O_3 and LiH were reacted in a LiCl melt at 750 ^oC. To the best to our knowledge this approach has since then been neglected, despite providing stoichiometric oxyhydrides in the gram scale. In this paper we go beyond the classically adopted routes for oxyhydride synthesis, and revisit the flux approach for preparation of La_2LiHO_3.

Kobayashi *et al*. have reported the existence of both orthorhombic (*Immm*) and tetragonal (*I*4/*mmm*) La_2LiHO_3 (RP type structure, $n = 1$), formed by direct reaction between La_2O_3 and LiH at high pressure (1 – 2 GPa) and intermediate temperatures (650 – 750 ^oC) [3]. In the orthorhombic polymorph the hydride- and oxide- anions in the perovskite block is arranged in an ordered manner, whereas in the tetragonal form the two species are disordered, Figure 1. According to Kobayashi *et al*., the obtained polymorph depends on the La_2O_3/LiH ratio used during synthesis as well as synthesis temperature and pressure. Currently, knowledge on thermal stability and decomposition products of La_2LiHO_3 is completely lacking. With applications in mind, for example electrochemical devices, such data are called for.

In this paper we report on the synthesis of La_2LiHO_3 by a flux method, reinvestigate its crystal structure in view of polymorphism as well as we explore the thermal stability along with characterizing decomposition products. Our studies are performed on phase pure samples using scanning electron microscopy (SEM), combined thermogravimetric analysis - differential scanning calorimetry - mass spectroscopy (TGA-DSC-MS), quasi elastic neutron scattering (QENS) combined with powder neutron diffraction (PND), X-ray diffraction (XRD) and *in situ* synchrotron radiation powder X-ray diffraction (SR-XRD) methods.

Experimental

La_2LiHO_3 was synthesized in LiCl (99.8 %, Cerac) flux with La_2O_3 (99.99 %, Molycorp) and LiH (95 %, Sigma Aldrich) as reactants, and by varying the molar ratio between 1:1 – 1:8 (for La_2O_3:LiH). The flux was kept between 600 °C and 750 °C, limited by the melting point of the flux and stability of the reactor vessel material. The flux was kept in a tantalum crucible inside a sealed stainless steel ampoule of an in-house build carousel [11], and heat treated for 6 - 48 hrs in a calibrated tube furnace. All starting materials were dried prior to use, and the reaction mixtures and Ta-crucible were prepared inside an Ar filled MBraun glovebox. After heat treatment, the ampoules were opened in air before LiCl and excess LiH was washed out with CH_3OH (99.8 %, VWR Chemicals). Due to the exothermic nature of the reaction between LiH and methanol, extra care was taken in this part of the synthesis. After completed washing, the samples were dried under vacuum and stored inside a glovebox. A deuterated sample used for PND was synthesized from LiD and washed with CH_3OD (both Sigma Aldrich). Further characterization were carried out on samples with a 1:4 La_2O_3:LiH ratio and 60 wt.% LiCl heated treated at 750 °C for 48 hours.

Combined Thermogravimetric Analysis (TGA) and Differential Scanning Calorimetry (DSC) measurements were carried out on a Netzsch STA 449 F1 Jupiter instrument coupled to a Mass Spectrometer (MS) for simultaneous TGA-DSC-MS analysis. The sample was heated from room temperature to 800 °C in O_2 (99.999 %, Praxair) using an Al_2O_3 crucible at a heating rate of 5 $^oC\ min^{-1}$. The buoyancy effect was corrected by subtracting a blank reference scan at exactly the same conditions.

A Hitachi SU 8230 field emission SEM was used to image particle morphology and size. Images of La_2LiHO_3 powder dispersed onto carbon tape on an Al-stub were obtained by collecting the secondary electrons produced by the electron beam with an acceleration voltage of 1.0 kV.

Home laboratory XRD data were collected on a Bruker AXS D8 Discover instrument with Cu $K\alpha_1$ radiation from a Ge(111) Johansson monochromator and a LynxEye strip detector. SR-XRD data were measured at BM01-A (Swiss-Norwegian Beam Lines) at ESRF in Grenoble, France, using the 2D Pilatus detector and a wavelength of 0.71210 Å for the 2θ-range 1.53 – 51.13°, collecting 3256 data points. The sample was heated in air in an open rotating quartz capillary with a diameter of 0.5 mm from room temperature to 700 °C at a heating rate of 2 ^{o}C min^{-1} and with a counting time of 20 seconds. Rietveld refinements were carried out using the *Topas v5* software [12].

PND experiments were carried out at the POLARIS instrument at ISIS pulsed neutron and muon source. The sample was measured for 3 h at room temperature in a thinwall vanadium 7 mm can. The data has been integrated using Mantid software [13] and the analysis was carried out in Jana2006 [14].

QENS measurements were performed on the IRIS neutron spectrometer at the ISIS pulsed neutron and muon source. Data were collected for temperatures ranging from 27 to 527 °C. Analysis was performed using the MANTID software [13]. The IRIS backscattering detectors were used as a diffraction bank to examine the correlation between structural and dynamic properties of the material by PND. The QENS signal was summed across all detectors and normalised by the total peak intensity. The resultant spectra were integrated over the energy range 0.05 – 0.6 meV (beyond the resolution function of IRIS), as a measure of the total change in QENS signal as a function of temperature, and this measured QENS signal is below referred to as "Γ_{QENS}".

Results and discussion

Synthesis, morphology and crystal structure:

La_2LiHO_3 is presently synthesized by reacting La_2O_3 and LiH in a LiCl melt following the procedure outlined by Schwarz [10]. Various synthesis conditions were explored and an overview can be found in Table S1. Quantities of up to 10 g were successfully synthesized in one batch. 1:1 ratio of La_2O_3:LiH resulted in a mixture between La_2O_3 and La_2LiHO_3, while all other conditions with surplus of LiH gave phase pure samples of La_2LiHO_3. Only the orthorhombic polymorph was obtained with no signs of the tetragonal variant. According to Kobayashi *et al*. the orthorhombic polymorph is expected to form in the temperature interval 650 – 750 °C at high pressures (1 – 2 GPa) for a La_2O_3:LiH ratio of 1:2. In our hands, reaction parameters such as flux temperature and quantity, La_2O_3:LiH molar ratio and reaction time did not affect the structural arrangement of the La_2LiHO_3 product. In contrast to Schwarz, who was able to synthesize phase pure La_2LiHO_3 only at 750 °C [10], we successfully obtained La_2LiHO_3 in the temperature interval 600 – 750 °C. SEM images of washed and dried La_2LiHO_3 shows well shaped single crystals with facets like truncated octahedrons and an average size of 10 × 10 × 10 μm^3, Figure 2. Optically, the crystals have a yellow translucent appearance.

The crystal structure of the orthorhombic polymorph was revisited by combining XRD and PND. Careful XRD analysis clearly documents La_2LiHO_3 to take a RP1 type structure with an orthorhombic distortion due to anion ordering relative to the tetragonal aristotype, as reported by Schwarz and Kobayashi *et al.* [3, 10]. The hydride anions are slightly smaller than oxide anions [15], and occupy the two opposite equatorial positions in the octahedron surrounding lithium, thereby shortening the *a*-axis of the unit cell and distorting it to an orthorhombic cell, Figure 1. Despite the fact that the Rietveld refinements of XRD patterns (Figure S1) were in good agreement with the reported structure, hydrogen and lithium positions are not accurately determined due to their insensitivity to X-rays in presence of the heavy lanthanum atom. For that reason a deuterated sample was measured by PND followed by Rietveld refinements. Using the crystallographic data extracted from the XRD refinements, the occupancy of all refined positions and the overall composition was found to be $La_2LiH_{0.255}D_{0.745}O_3$, confirming the presence of hydride anion in the compound. The occupancies of deuterium and hydrogen were locked to keep the overall occupancy of the H/D position to 1 whereas all other occupancies (La, Li, O1, O2) were refined and found to be 1. Relevant obtained structural data from the PND refinements are reported in Table 1, and the experimental and refined neutron diffraction pattern is shown in Figure S2. The impurity phase $La(OH)_3$ was included into the refinement [16]. The final composition in mass fraction is $La_3LiH_{0.255(1)}D_{0.745(1)}O_3$ 99.40(1) % and $La(OH)_3$ 0.60(1) %.

Thermal stability:

As-synthesized samples degrade slowly in air, and XRD experiments shows $La(OH)_3$ formation after air exposure overnight and full decomposition in about one week. This observation is not surprising as hydrogen in general has a preference to be in oxidation state +1 rather than –1, and air is and oxidant. Combined TGA-DCS-MS, and *in situ* SR-XRD were therefore used to describe the thermal stability of La_2LiHO_3. In addition QENS data was used to correlate how changes in hydride dynamics affect the structure/chemical nature of the system.

Results from a typical TGA-DCS-MS heating experiment in O_2-atmosphere are reported in Figure 3. At 450 – 590 °C a significant mass gain is observed in the TGA, followed by release of water and an exothermic DSC signal. This mass change corresponds indeed well with the expected increase for oxidation of the oxyhydride to oxide; *i.e*. La_2LiHO_3 to $La_2LiO_{3.5}$ (2.1 % mass change), where formally one hydride anion is replaced by one half oxide anion and one half oxygen vacancy. In sum the TGA and MS results prove the presence of hydride anions. It should be noted that a slower heating rate (reduced from 5 to 1 $^oC\ min^{-1}$) did not change the on-set temperature of the oxidation, however, at these conditions the oxidation took place over a more narrow temperature range, 450 – 565 °C.

The TGA curve reported in Figure S3 shows two minor mass losses in the temperature intervals 230 – 290 °C and 330 – 390 °C for a sample exposed to air before the experiment. According to MS and DSC these losses are accompanied by the release of water and weak endothermic responses. We attribute these minor changes to a two-step decomposition of surface $La(OH)_3$ [$La(OH)_3 \rightarrow LaOOH \rightarrow La_2O_3$] [17], originating from mild oxidation of the

sample when exposed to air (see SR-XRD analysis below, not visible with home laboratory XRD). This is strongly corroborated by the QENS data (Figure 4), showing a drop in signal at these temperatures, which is consistent with a loss of hydrogenous species.

The QENS data gives additional insight to the oxidation process, showing a large and systematic boost in the QENS signal as the sample approaches the decomposition temperature (Figure 4). This change in the QENS signal is probably caused by increased diffusivity of the hydride ions with temperature. Given the energy resolution of the IRIS instrument it is not possible to perform an unambiguous Lorentzian fitting to establish a quantitative value for the diffusion coefficient. However, it is clear that the increased mobility of the hydride ions is likely to be the main cause for facilitating the oxidation of La_2LiHO_3. The increased hydride mobility allows the hydride anions to diffuse to the surface, which is anticipated to facilitate the oxidation process. The PND data from IRIS shows no structural changes in the structure, displaying a steady increase in lattice parameters over the studied temperature range (Figure 5). I.e., the *in situ* PND data provide evidence that we observe increased mobility of hydride anions within the same primary crystal structure with increased temperatures.

In situ SR-XRD (open quartz capillary) was used to map structural changes during oxidation and thereby complement the TGA-DSC-MS data, see Figure 6. The small quantities of surface $La(OH)_3$ caused by exposure to humidity and oxygen, decomposed in two steps; first into LaOOH at 210 – 225 °C and thereafter into La_2O_3 at 305 – 330 °C. The oxyhydride La_2LiHO_3 starts to oxidize at about 450 °C and the structurally related $La_2LiO_{3.5}$ appears. The oxidation continues to around 600 °C, implying a quite slow oxidation process (heating rate 2 $^oC\ min^{-1}$). Note that formation of $La(OH)_3$ is not observed under decomposition of La_2LiHO_3 and is therefore not assumed to be a primary decomposition product. The evolution of the lattice parameters of orthorhombic La_2LiHO_3 during heating is reported in Figure 7. Below 350 ^oC all lattice parameters expand in a monotonic manner. However, above 350 °C the *a*- and *b*- lattice parameters start slowly approaching each other, indicating that the oxidation reduces the degree of the orthorhombic distortion, see *a*/*b* ratio in Figure 7. This structural change does not correlate with any mass changes in the TG experiments, and hence not with any changes in the H/O ratio of the oxyhydride. Note the limited number of data points for the PND data makes the temperature induces lattice changes less evident.

It should be pointed out that La_2LiHO_3 shows good thermal stability in oxygen (~450 ^oC), similar to oxyhydrides as $ATiH_xO_{3-x}$ (A = Ca, Sr, Ba) (380 – 460 °C) [18], and better than $SrCrHO_2$ [9] (170 °C).

High temperature derivatives – crystal structure of $La_2LiO_{3.5}$:

The oxidation of La_2LiHO_3 results according to TGA-DSC-MS and XRD in formation of $La_2LiO_{3.5}$. Attfield and Férey described $La_2LiO_{3.5}$ to take a tetragonal K_2NiF_4-type structure (*I*4/*mmm*) with partial occupancy of the equatorial oxygen position (75 %) [19]. The present XRD data show immediately that reflection like (110), (112) and (114) were split (see insert to Figure S4), and hence not compatible with a tetragonal model. The splitting of the (11*l*)-family of reflection indicates a distortion along the cell diagonals of the tetragonal cell. Using

ISODISORT [20], an orthorhombic supercell along the diagonals of the tetragonal cell with a basis [(1,1,0),(1,–1,0),(0,0,1)] were chosen with space group *Fmmm*, and refined to have slightly different a_O and b_O parameters [a_O = 5.196(6) Å, b_O = 5.136(7) Å]. In accordance with Attfield and Férey [19], we observed partial occupancy on the equatorial oxygen position and no vacancies at the axial oxygen position. The crystal structure of $La_2LiO_{3.5}$ is visualized in Figure S5 and the tetragonal and orthorhombic cells are illustrated in Figure S6. Refined structural parameters for $La_2LiO_{3.5}$ are reported in Table 2, and the Rietveld profile fit is shown in Figure S4. The additional reflections seen from La_2O_3 originate from a partial decomposition of $La_2LiO_{3.5}$.

Structural aspects La_2LiHO_3 – $La_2LiO_{3.5}$:
The thermal expansion of the lattice parameters of La_2LiHO_3, Figure 7, showed an anomalous behavior (not connected to any mass change) for the orthorhombic distortion in terms of *a*/*b* ratio at temperatures above 350 ^oC. However, still at the thermal stability limit the *a*/*b* ratio remains far below one; *i.e.* the value for a tetragonal symmetry. This is also supported by PND at elevated temperatures where no symmetry change was observed. This strongly indicates that the tetragonal La_2LiHO_3 reported by Kobayashi *et al.* [3] cannot reflect a stoichiometric sample. Hence, other factors must be in play.

In this respect one may consider the possible existence of a solid solution, $La_2LiH_{1-x}O_{3+x/2}$, with La_2LiHO_3 (x = 0) and $La_2LiO_{3.5}$ (x = 1) as the two end members where one hydride anion is substituted by one half oxide anion and one half vacancy. Figure 8 shows the unit cell volumes of these two orthorhombic end-members according to current results, and a stippled line for a potential Vegard law relationship. Figure 8 includes the unit cell volume for the tetragonal variant reported by Kobayashi *et al.* [3]. This value is significantly larger than the volume currently observed for the ordered orthorhombic La_2LiHO_3 variant. Since our high temperature SR-XRD data show no sign of a transition into a tetragonal phase prior to thermal decomposition, our data suggests that the tetragonal variant is indeed partly oxidized, with oxide anions replacing hydride anions under formation of oxygen vacancies, □:

$$La_2LiHO_3(s) + \frac{x}{2}\ O_2(g) \rightarrow La_2LiH_{1-x}O_{3+\frac{x}{2}}\square_{\frac{x}{2}}(s) + \frac{x}{2}\ H_2O(g)$$

By considering the V(H/O ratio) curve in Figure 8, the unit cell volume of the tetragonal phase would correspond to an H/O composition of approximately 0.13, *i.e.* to $La_2LiH_{0.43}O_{3.28}\square_{0.28}$. This analysis is fully in line with the formula suggested by Kobayashi *et al*. of $La_2LiH_{0.53}O_{3.21}\square_{0.26}$ for the tetragonal phase.

Concluding remarks

La_2LiHO_3 belongs to the family of oxyhydrides in which oxide- and hydride- anions share the same anionic lattice. These compounds are rare and exotic in nature. Currently we have revisited the alkali flux method and report in detail on conditions favouring high quality high yield samples of La_2LiHO_3. This route allows production of larger quantity (up to 10 g is synthesized in this work) of material relative to most routes otherwise adopted for this family

of compounds. Thereby sufficient quantities of materials become available for wider property studies and benchmarking.

In the literature a tetragonal variant is reported along with the currently explored orthorhombic polymorph. Within the current synthesis window the tetragonal phase was not obtained. Based on SR-XRD and considerations of unit cell volumes per formula number, we currently suggest that the stoichiometric La_2LiHO_3 is orthorhombic throughout its stability range up to decomposition at around 450 ^oC, whereas the tetragonal variant may represent a slightly oxidized variant, tentatively $La_2LiH_{0.43}O_{3.28}\square_{0.28}$ with $\square$ denoting an anion vacancy of the Ruddlesden Popper $n = 1$ type phase.

La_2LiHO_3 decompose in an oxygen atmosphere at ~450 ^oC to $La_2LiO_{3.5}$. It is likely that high mobility of hydride anions close to the decomposition temperature is a main factor for inducing the oxidation reaction. The crystal structure of $La_2LiO_{3.5}$ is revisited, and is shown to take an RP1 type structure with an orthorhombic distortion with space group *Fmmm*.

Acknowledgements

This work is part of activities in the FOXHOUND project, funded by The Faculty of Mathematics and Natural Sciences, University of Oslo via the Strategic Research Initiative program. The authors gratefully acknowledge the use of the Norwegian Center for X-ray Diffraction, Scattering and Imaging (RECX) and gratefully acknowledged the staff at the Swiss-Norwegian Beam Lines (SNBL), ESRF, France, for technical support. We also acknowledge ISIS neutron and muon source for beamtime (POLARIS and IRIS instrument).

Supporting Information:

Table providing relevant synthesis parameters, XRD and PND patterns of La_2LiHO_3, TGA-DSC-MS of air exposed La_2LiHO_3 sample, XRD pattern of $La_2LiO_{3.5}$, schematics showing the crystal structure of $La_2LiO_{3.5}$.

Author Information:

*E-mail: a.o.sjastad@kjemi.uio.no.

Notes:

The authors declare no competing financial interest.

References:

1. Phair, J. W.; Badwal, S. P. S., Review of proton conductors for hydrogen separation. *Ionics* **2006,** *12*, 103-115.
2. Sakintuna, B.; Lamari-Darkrim, F.; Hirscher, M., Metal hydride materials for solid hydrogen storage: A review. *Int. J. Hydrogen Energy* **2007,** *32*, 1121-1140.
3. Kobayashi, G.; Hinuma, Y.; Matsuoka, S.; Watanabe, A.; Iqbal, M.; Hirayama, M.; Yonemura, M.; Kamiyama, T.; Tanaka, I.; Kanno, R., Pure H^- conduction in oxyhydrides. *Science* **2016,** *351*, 1314-1317.
4. Kobayashi, Y.; Hernandez, O. J.; Sakaguchi, T.; Yajima, T.; Roisnel, T.; Tsujimoto, Y.; Morita, M.; Noda, Y.; Mogami, Y.; Kitada, A.; Ohkura, M.; Hosokawa, S.; Li, Z.; Hayashi, K.; Kusano, Y.; Kim, J. e.; Tsuji, N.; Fujiwara, A.; Matsushita, Y.; Yoshimura, K.; Takegoshi, K.; Inoue, M.; Takano, M.; Kageyama, H., An oxyhydride of $BaTiO_3$ exhibiting hydride exchange and electronic conductivity. *Nat. Mater.* **2012,** *11*, 507-511.
5. Denis Romero, F.; Leach, A.; Möller, J. S.; Foronda, F.; Blundell, S. J.; Hayward, M. A., Strontium Vanadium Oxide–Hydrides: "Square-Planar" Two-Electron Phases. *Angew. Chem., Int. Ed.* **2014,** *53*, 7556-7559.
6. Bang, J.; Matsuishi, S.; Hiraka, H.; Fujisaki, F.; Otomo, T.; Maki, S.; Yamaura, J.-i.; Kumai, R.; Murakami, Y.; Hosono, H., Hydrogen Ordering and New Polymorph of Layered Perovskite Oxyhydrides: $Sr_2VO_{4-x}H_x$. *J. Am. Chem. Soc.* **2014,** *136*, 7221-7224.
7. Hayward, M. A.; Cussen, E. J.; Claridge, J. B.; Bieringer, M.; Rosseinsky, M. J.; Kiely, C. J.; Blundell, S. J.; Marshall, I. M.; Pratt, F. L., The Hydride Anion in an Extended Transition Metal Oxide Array: $LaSrCoO_3H_{0.7}$. *Science* **2002,** *295*, 1882-1884.
8. Bridges, C. A.; Darling, G. R.; Hayward, M. A.; Rosseinsky, M. J., Electronic Structure, Magnetic Ordering, and Formation Pathway of the Transition Metal Oxide Hydride $LaSrCoO_3H_{0.7}$. *J. Am. Chem. Soc.* **2005,** *127*, 5996-6011.
9. Tassel, C.; Goto, Y.; Kuno, Y.; Hester, J.; Green, M.; Kobayashi, Y.; Kageyama, H., Direct Synthesis of Chromium Perovskite Oxyhydride with a High Magnetic-Transition Temperature. *Angew. Chem., Int. Ed.* **2014**, 10377-10380.
10. Schwarz, H., Neuartige Hydrid-Oxide der Seltenen Erden: Ln_2LiHO_3 mit Ln = La, Ce, Pr und Nd. *Karlsruhe*, 1991.
11. Fjellvåg, Ø. S., Fjellvåg; H.; Sjåstad, A. O., Hydride oxides, a new material class of complex mixed anion compounds, *Proceedings of the Internation Conference on Adcances in Functional Materials*, Chennai, P. Ravindran, R. V., Ed. Chennai, 2017; 261-262.
12. Bruker-AXS, TOPAS V5: General profile and structure analysis software for powder diffraction data. - User's Manual, *Bruker AXS, Karlsruhe, Germany.*, 2013.
13. Arnold, O.; Bilheux, J. C.; Borreguero, J. M.; Buts, A.; Campbell, S. I.; Chapon, L.; Doucet, M.; Draper, N.; Ferraz Leal, R.; Gigg, M. A.; Lynch, V. E.; Markvardsen, A.; Mikkelson, D. J.; Mikkelson, R. L.; Miller, R.; Palmen, K.; Parker, P.; Passos, G.; Perring, T. G.; Peterson, P. F.; Ren, S.; Reuter, M. A.; Savici, A. T.; Taylor, J. W.; Taylor, R. J.; Tolchenov, R.; Zhou, W.; Zikovsky, J., Mantid—Data analysis and visualization package for neutron scattering and SR experiments. *Nucl. Instrum. Methods Phys. Res., Sect. A* **2014,** *764*, 156-166.
14. Petříček, V.; Dušek, M.; Palatinus, L., Crystallographic Computing System JANA2006: General features. In *Z. Kristallogr.* 2014; Vol. 229, p 345-352.
15. Lang, P. F.; Smith, B. C., Ionic radii for Group 1 and Group 2 halide, hydride, fluoride, oxide, sulfide, selenide and telluride crystals. *Dalton Trans.* **2010,** *39*, 7786-7791.
16. Khidirov, I.; Om, V. T., Localization of hydrogen atoms in rare earth metal trihydroxides $R(OH)_3$. *Phys. Status Solidi A* **1993,** *140*, K59-K62.

17. Yamamoto, O.; Takeda, Y.; Kanno, R.; Fushimi, M., Thermal decomposition and electrical conductivity of $M(OH)_3$ and MOOH (M=Y, lanthanide). *Solid State Ionics* **1985,** *17*, 107-114.
18. Sakaguchi, T.; Kobayashi, Y.; Yajima, T.; Ohkura, M.; Tassel, C.; Takeiri, F.; Mitsuoka, S.; Ohkubo, H.; Yamamoto, T.; Kim, J. e.; Tsuji, N.; Fujihara, A.; Matsushita, Y.; Hester, J.; Avdeev, M.; Ohoyama, K.; Kageyama, H., Oxyhydrides of (Ca,Sr,Ba)TiO_3 Perovskite Solid Solutions. *Inorg. Chem.* **2012,** *51*, 11371-11376.
19. Attfield, J. P.; Férey, G., Preparation and crystal structures of $La_2Cu_{1-x}Li_xO_4$ solid solutions and evidence for a new oxide with a defect K_2NiF_4 structure: $La_4Li_2O_7$. *J. Solid State Chem.* **1989,** *80*, 112-119.
20. Stokes, H. T.; Hatch, D. M.; Campbell, B. J.; Tanner, D. E., ISODISPLACE: a web-based tool for exploring structural distortions. *J. Appl. Crystallogr.* **2006,** *39*, 607-614.

Tables:

Table 1: Crystallographic data of $La_2LiD_{0.745}H_{0.255}O_3$ in space group *Immm* [*a* = 3.571521(41) Å, *b* = 3.763532(44) Å, *c* = 12.97854(15) Å] from PND. U_{iso} corresponds to the thermal displacement parameter.

Atom	*Wyckoff*	*x*	*y*	*y*	*Occupancy*	U_{iso}
La	4i	0	0	0.363344(21)	1	0.00903(7)
Li	2a	0	0	0	1	0.01553(34)
D	2b	0.5	0	0	0.745(1)	0.02343(28)
H	2b	0.5	0	0	0.255(1)	0.02343(28)
O1	4i	0	0	0.176738(31)	1	0.01216(9)
O2	2d	0.5	0	0.5	1	0.01216(9)

Table 2: Crystallographic data of $La_2LiO_{3.5}$ in space group *Fmmm* [*a* = 5.196(6) Å, *b* = 5.136(7) Å, *c* = 13.279(7) Å] from XRD. Same values for the atomic displacement parameters were used for lithium and oxygen atoms. U_{iso} corresponds to the thermal displacement parameter.

Atom	*Wyckoff*	*x*	*y*	*y*	*Occupancy*	U_{iso}
La	8i	0.5	0.5	0.637(7)	1	0.019(3)
Li	4a	0	0.5	0.5	1	0.02(2)
O1	8i	0.5	0.5	0.825(0)	1	0.02(2)
O2	8e	0.25	0.25	0.5	0.75	0.02(2)

Figures

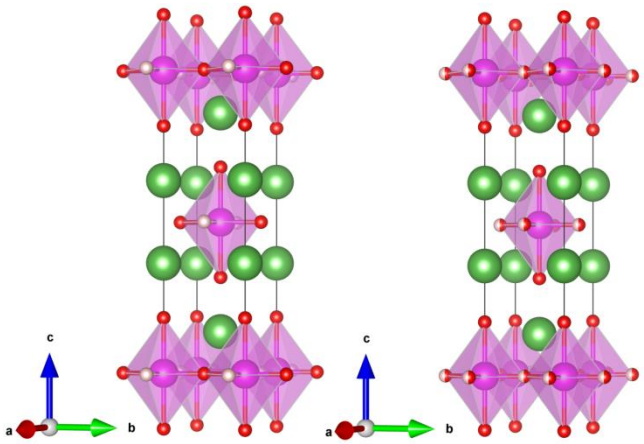

Figure 1: Crystal structure of orthorhombic (*Immm*) La_2LiHO_3 (left) and tetragonal (*I4/mmm*) La_2LiHO_3 (right). The atoms are lanthanum (green), lithium (pink), hydrogen (white) and oxygen (red). Note the split occupancy between hydrogen and oxygen on the equatorial position (half red – half white spheres).

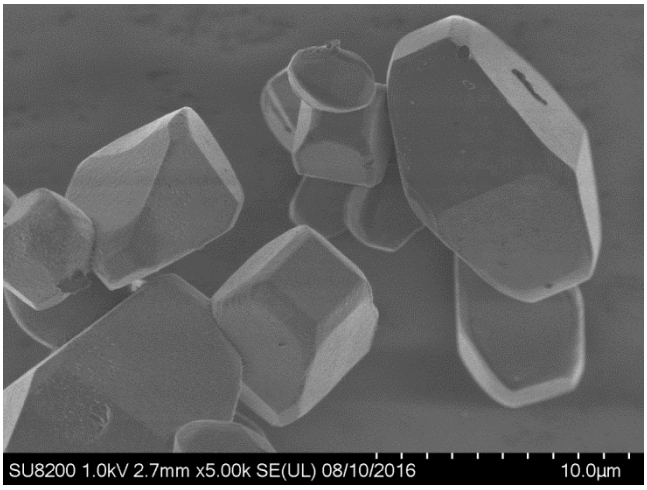

Figure 2: SEM image of La_2LiHO_3 single crystals after drying and washing.

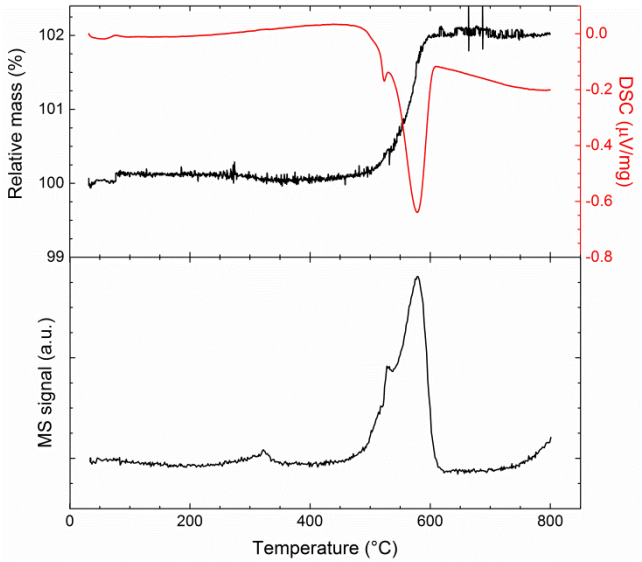

Figure 3: Combined TGA, DSC (top) and MS (bottom) of La_2LiHO_3 heated in O_2 (5 ^oC min^{-1}). The large mass change is the oxidation of La_2LiHO_3 to $La_2LiO_{3.5}$, and is accompanied by an exothermic signal in DSC and identified as water by MS.

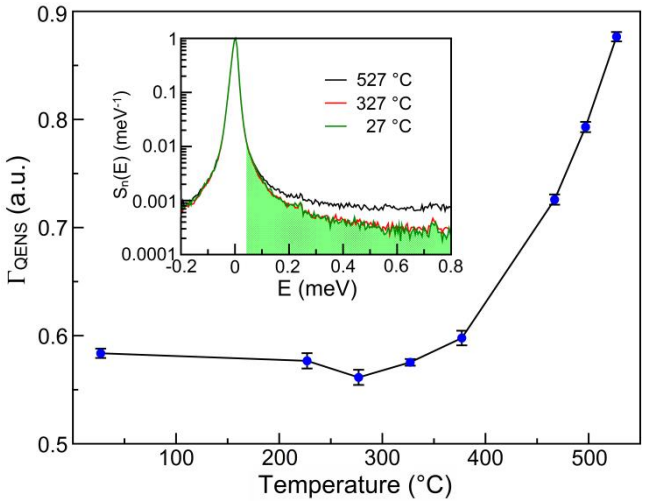

Figure 4: The main plot shows the integral of the "detector summed" and normalized QENS signal within the energy range 0.04 – 0.8 meV (green shaded region) as a function of temperature. Inset: The QENS spectra at three representative temperatures, 27 °C (green), 327 °C (red) and 527 °C (black). See definition of Γ_{QENS} in the experimental section.

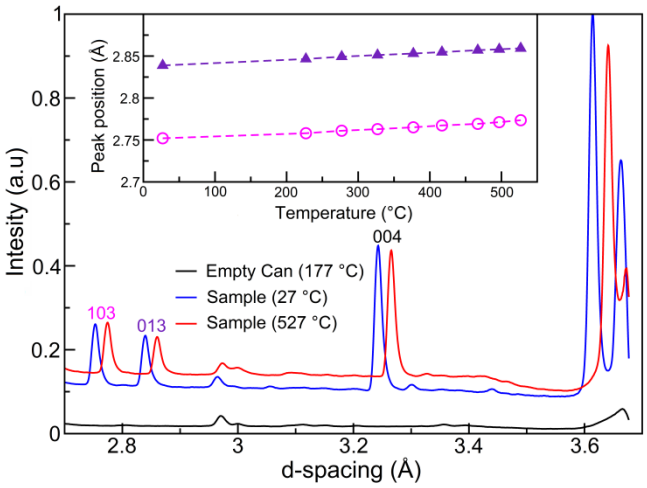

Figure 5: Main plot: PND measurements performed *in situ* during the QENS measurements for the sample at 27 °C (blue), 527 °C (red) and for the empty sample can. The evolution of the peak position of the (103)-reflection (pink) and (013)-reflection (purple) is shown in the inset.

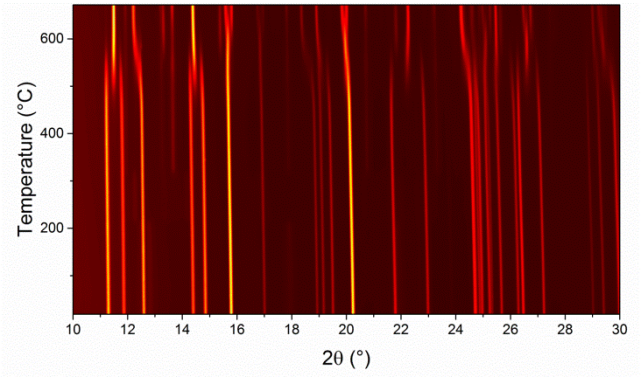

Figure 6: *In situ* heating of La_2LiHO_3 in an open quartz capillary heated with a rate of 2 ^{o}C min^{-1}. The oxidation of La_2LiHO_3 is starting at about 450 °C. The decomposition $La(OH)_3 \rightarrow LaOOH \rightarrow La_2O_3$ is weakly visible at 13 – 14°.

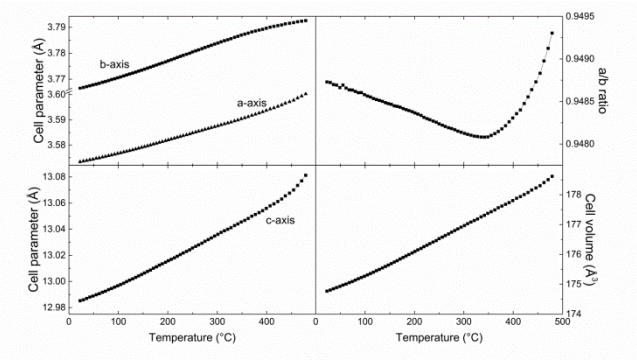

Figure 7: Evolution of lattice parameters of La_2LiHO_3 under heating from room temperature to 480 °C in an open capillary heated with a rate of 2 ^{o}C min^{-1}.

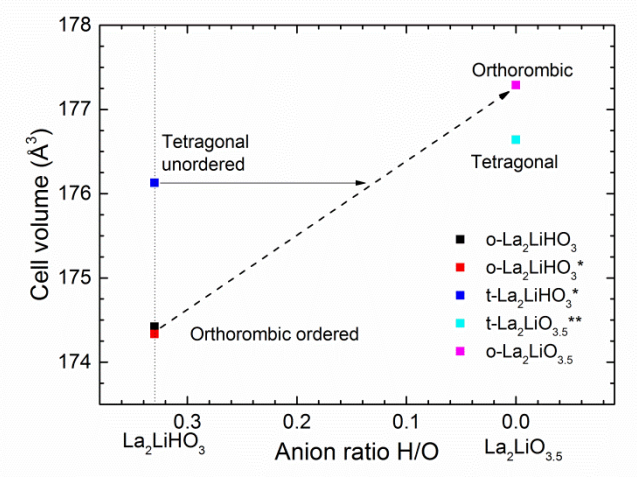

Figure 8: Illustration of Vegard's law for the change in unit cell volume for oxidation of La_2LiHO_3 to $La_2LiHO_{3.5}$. Lattice parameters for * is from [3], ** from [19], others from this work. "o" and "t" refers to orthorhombic and tetragonal structures.

For Table of Contents Only:

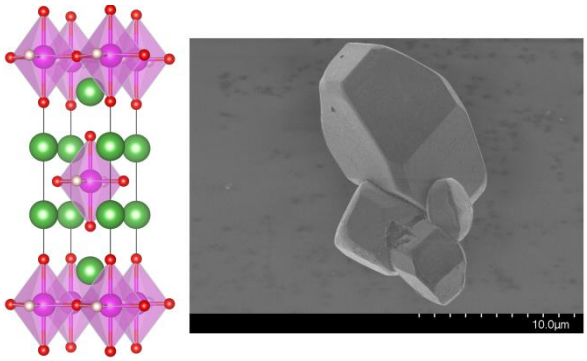

Synopsis:

The orthorhombic oxyhydride La_2LiHO_3 has been synthesized as small single crystals by an unexplored halide flux method which favors high quality samples. The route opens up for gram scale samples and synthesis of new oxyhydrides. The crystal structure, thermal stability and intermediate decomposition products are investigated in detail.